ADVANCED FUNCTIONAL MATERIALS
www.afm-journal.de

pH-Responsive, Light-Triggered on-Demand Antibiotic Release from Functional Metal–Organic Framework for Bacterial Infection Combination Therapy

*Zhiyong Song, Yang Wu, Qi Cao, Huajuan Wang, Xiangru Wang, and Heyou Han**

To satisfy the ever-growing demand in bacterial infection therapy and other fields of science, great effort is being devoted to the development of methods to precisely control drug release and achieve targeted use of an active substance at the right time and place. Here, a new strategy for bacterial infection combination therapy based on the light-responsive zeolitic imidazolate framework (ZIF) is reported. A pH-jump reagent is modified into the porous structure of ZIF nanoparticles as a gatekeeper, allowing the UV-light (365 nm) responsive in situ production of acid, which subsequently induces pH-dependent degradation of ZIF and promotes the release of the antibiotic loaded in the mesopores. The combination of the UV-light, the pH-triggered precise antibiotic release, and the zinc ions enables the light-activated nanocomposite to significantly inhibit bacteria-induced wound infection and accelerate wound healing, indicating a switchable and synergistic antibacterial effect. The light irradiated accumulation of acid ensures the controlled release of antibiotic and controlled degradation of ZIF, suggesting the therapeutic potential of the metal–organic frameworks-based smart platform for controlling bacterial infection.

1. Introduction

Bacterial infection is a primary cause of morbidity and mortality worldwide despite the widespread use of broad-spectrum antibiotics.[1] The major problems for antibiotic therapy are drug resistance or adverse effects, but controlled drug-release systems have the potential to reduce side effects and achieve targeted use of an active substance at the right time and place.[2] In particular, drug release mechanisms with triggers that respond to surrounding factors, such as pH,[3] temperature,[4] illumination,[5] and enzymes[6] are of high practical significance. Toward this goal, various nanomaterials including nanoparticles,[7] microgels,[8] nanotubes,[9]polymeric micelles,[10] and fluorescent probe[11] are or can be designed to be particularly sensitive to environmental factors.

Metal–organic frameworks (MOFs), as a new type of miniature crystalline porous material, have been extensively studied.[12] These materials act as effective nanoparticle-based delivery platforms and have shown great potential for biomedical applications due to their combined benefits of nanostructures and the intrinsic properties of bulk crystalline MOFs, such as controllable composition, high porosity, large surface area, intrinsic biodegradability as a result of relatively labile metal–ligand bonds, versatile functionality, and good biocompatibility.[13] The zeolitic imidazolate framework-8 (ZIF-8) is a subclass of MOFs, formed by coordination between Zn^{2+} ions and 2-methylimidazole (HmIm), with high surface area and negligible cytotoxicity. The largest pore size in the ZIF-8 structure has a diameter of ≈11.6 Å interconnected by 6-ring windows of a diameter of 3.40 Å.[14] ZIFs have been used in gas separation,[15] catalysts,[16] and as carriers for metal nanoparticles[17] and drugs.[18] Additionally, ZIF-8 is stable under physiological conditions and decomposable under acidic conditions, which can be used to construct pH-sensitive drug delivery systems.[12a,19]

Currently, to satisfy the ever-growing demand in controllable drug release, different strategies have been developed to implement the gatekeeper concept.[20] The gatekeeper consisting of stimulus-responsive functional components can be used as the blocking caps to control opening/closing of pore entrances and respond to external agents and conditions.[21] However, the installation of stimulus-responsive functional groups onto the surface of nanoparticles requires complicated synthetic steps. Several steps of the post functionalization of drug-loaded nanoparticles resulted in the leakage of the cargo.[21a,22]

Herein, we report a simple and robust method for one-pot synthesis of a novel gatekeeper nanocomposite for light-controlled antibacterial therapy based on a 2-nitrobenzaldehyde (o-NBA) modified MOF, designated as o-NBA@ZIF-8. The

Dr. Z. Y. Song, Y. Wu, Prof. H. Y. Han
State Key Laboratory of Agriculture Microbiology
College of Science
Huazhong Agricultural University
Wuhan 430070, China
E-mail: hyhan@mail.hzau.edu.cn
Q. Cao, Dr. X. R. Wang
State Key Laboratory of Agricultural Microbiology
College of Veterinary Medicine
Huazhong Agricultural University
Wuhan 430070, China
H. J. Wang, Prof. H. Y. Han
State Key Laboratory of Agriculture Microbiology
College of Food Science and Technology
Huazhong Agricultural University
Wuhan 430070, China

DOI: 10.1002/adfm.201800011

strategy consists of i) preparing ZIF-8, ii) installing "light responsive" o-NBA (a pH-jump reagent) into the mesopores of ZIF-8 that act as "gatekeeper," and iii) loading the antibacterial agent rifampicin (RFP) into the mesopores (RFP&o-NBA@ZIF-8). Under light treatment, the sequential reaction can induce the pH-dependent degradation of MOF in the designed gatekeeper system, and the RFP loaded in the mesopores can be released in a controllable fashion. In addition, using both regular and Methicillin-resistant *Staphylococcus aureus* (MRSA), we demonstrated that a synergistic antibacterial and cure effect could be achieved by a rational combination of drugs and scaffold materials to promote the healing speed of the wound.

2. Results and Discussion

2.1. Synthesis and Characterization of RFP&o-NBA@ZIF-8

In the present work, the RFP&o-NBA@ZIF-8, RFP@ZIF-8, and o-NBA @ZIF-8 were first synthesized and the detailed synthetic procedure was presented in the Experimental Section. The transmission electron microscopy (TEM) image confirmed that a porous structure was obtained (**Figure 1**a). While the morphology of crystals did not obviously change with the addition of RFP and o-NBA, the particle size increased and the size distribution broadened (from 144.9 ± 4.2 to 189.7 ± 3.0 nm) as shown by dynamic light scattering (DLS; Figure S1, Supporting Information). To confirm that the RFP and o-NBA were embedded in the ZIF-8 crystals, the nitrogen adsorption–desorption isotherms of pure ZIF-8 and RFP&o-NBA@ZIF-8 were measured at 77 K (Figure S2, Supporting Information). The resulting BET surface areas of pure ZIF-8 and RFP&o-NBA@ZIF-8 were 393.23 and 155.05 m^2 g^{-1}, respectively, which was consistent with the presence of RFP and o-NBA. The samples were also tested by the X-ray diffraction (XRD) and Fourier-transform infrared (FT-IR) spectroscopy (Figure 1). XRD results showed that the RFP&o-NBA@ZIF-8 particles were of high crystallinity with sharp diffraction peaks (Figure 1b). The decrease of the peak intensity at the low angles for ZIF-8 with RFP or o-NBA loadings was due to the presence of RFP or o-NBA molecules in the pores of ZIF-8 crystals. No diffraction peaks were observed from the RFP or o-NBA molecules, indicating that no RFP or o-NBA crystals were present in the RFP&o-NBA@ZIF-8, RFP@ZIF-8, and o-NBA@ZIF-8 materials. Additionally, several bands were observed for ZIF-8 in the FT-IR spectrum. As shown in Figure 1c, the absorption bands at 422, 500–1350, and 1350–1500 cm^{-1} were attributed to Zn—N stretching mode, the plane bending and stretching of imidazole ring, respectively.[23] The absorption peaks at 3138 and 2933 cm^{-1} in the spectra of the ZIF-8 and ZIF-8 complex were due to the stretching vibrations of C—H bonds in the methyl group and the imidazole ring. Meanwhile, the TEM elemental mappings indicated the uniform distribution of Zn, N, and O elements in the same particle, which also evidenced the presence of RFP and o-NBA in the nanoparticles as the N and O atoms shown in Figure 1d. Furthermore, the energy dispersive spectroscopy pattern (Figure S3, Supporting Information) proved the similar results. Thermogravimetric analysis (Figure S4, Supporting Information) revealed that the maximum weight loss occurred at around 150–700 °C, which corresponded to the decomposition of RFP and o-NBA, indicating that RFP and o-NBA were embedded in the ZIF-8. UV–vis result also agreed with the loading rate of RFP and o-NBA in the ZIF-8 (Table S1, Supporting Information). All the particles were highly

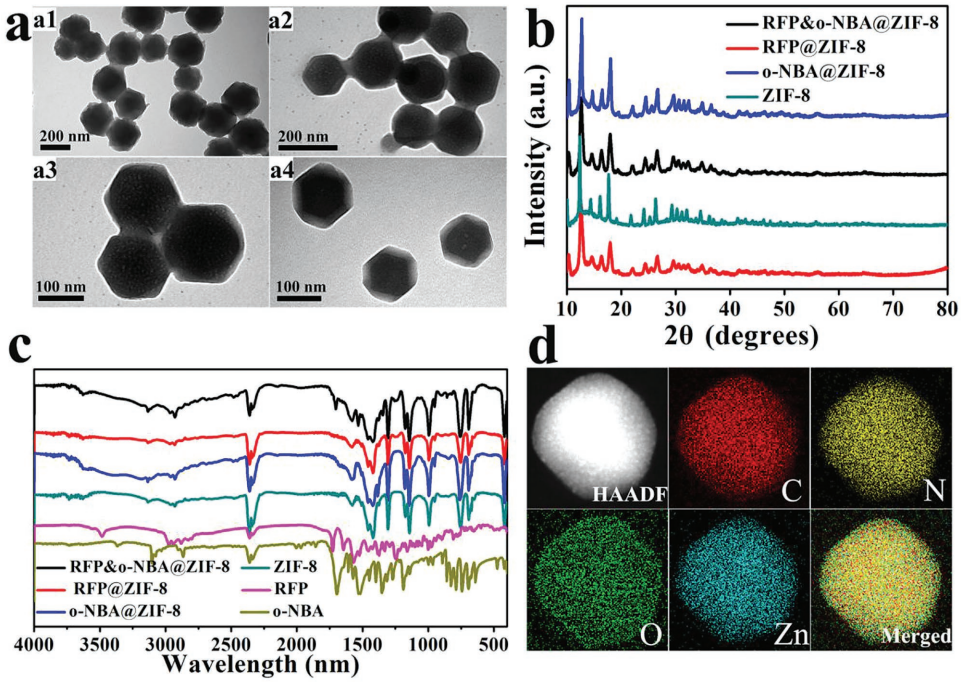

Figure 1. a) TEM characterization of (a-1) RFP&o-NBA@ZIF-8, (a-2) RFP@ZIF-8, (a-3) o-NBA@ZIF-8, and (a-4) ZIF-8; b) XRD, c) FT-IR, and d) mapping of single nanoparticle of RFP&o-NBA@ZIF-8.

dispersed and stable in water and phosphate-buffered saline (PBS) (pH 7.4), due to their high ζ potentials (+30.5, −14.0, +35.0, +25, and +27 mV for ZIF-8, RFP, o-NBA@ZIF-8, RFP@ZIF-8, and RFP&o-NBA@ZIF-8, respectively) (Figure S5, Supporting Information). The effect on the cell proliferation and cytotoxicity of the RFP&o-NBA@ZIF-8 was evaluated by the widely established methyl thiazolyl tetrazolium (MTT) assay, and the results suggested that the RFP&o-NBA@ZIF-8 had no signs of toxicity (Figure S6, Supporting Information).

2.2. Light-Induced pH-Dependent Degradation of MOF

In our design, the light-responsive degradation of MOF was critical in creating a light-triggered RFP controlled release system. First, the photoresponsive dissolution property of o-NBA@ZIF-8 was evaluated under light irradiation (365 nm, 5.25 mw cm^{-2}). The results showed that the crystallinity of o-NBA@ZIF-8 started to be gradually dissolved after irradiation for 30 min, and the material thoroughly lost its original structure in solution after 150 min (Figure S7, Supporting Information), suggesting that o-NBA@ZIF-8 has a photoresponsive property, which could be exploited as a controlled release vector to deliver an engineered drug. Furthermore, the RFP&o-NBA@ZIF-8 showed the similar pH-dependent degradation ability to that of o-NBA@ZIF-8 when irradiated by light (**Figure 2**a). However, we observed that the presence of RFP reduces the RFP&o-NBA@ZIF-8 response to light irradiation, which was ascribed to the pH changes in the ZIF-8 environment when undergoing intramolecular excited-state hydrogen transfer upon light irradiation, leading to different light responses (Figure S8, Supporting Information). To further confirm the dissolution of RFP&o-NBA@ZIF-8 under illumination conditions, we tested the pH and release effect of Zn^{2+} based on a different illumination time. In Figure 2b, it can be seen that, with the extension of illumination time, the pH of RFP&o-NBA@ZIF-8 in the solution showed an obvious change, while under dark treatment, the pH of the RFP@ZIF-8 and RFP&o-NBA@ZIF-8 remained almost unchanged. The o-NBA as a pH-jump reagent is incorporated onto nano o-NBA@ZIF-8 as a gatekeeper, which is known to lower the pH of the environment when undergoing intramolecular excited-state hydrogen transfer (ESHT) upon light irradiation and proceed *via* a bicyclic benzisoxazolidine intermediate to afford 2-nitrosobenzoic acid and proton.[24] In Figure 2c, the Zn^{2+} release efficiency for RFP&o-NBA@ZIF-8 reached a maximum of 90 wt% in 150 min under UV light exposure (5.25 mw cm^{-2}), while the release efficiency under dark treatment reached 60 wt% which may contribute to the acid zinc indicator (pH 5.3) (Figure S9, Supporting Information). The similar Zn^{2+} release efficiency results were also obtained by the atomic absorption spectroscopy (AAS) assay (Figure S10, Supporting Information). These results implicated that the o-NBA can lower the pH of the environment to destroy the MOF structure upon light irradiation, leading to the significant release of Zn^{2+}.

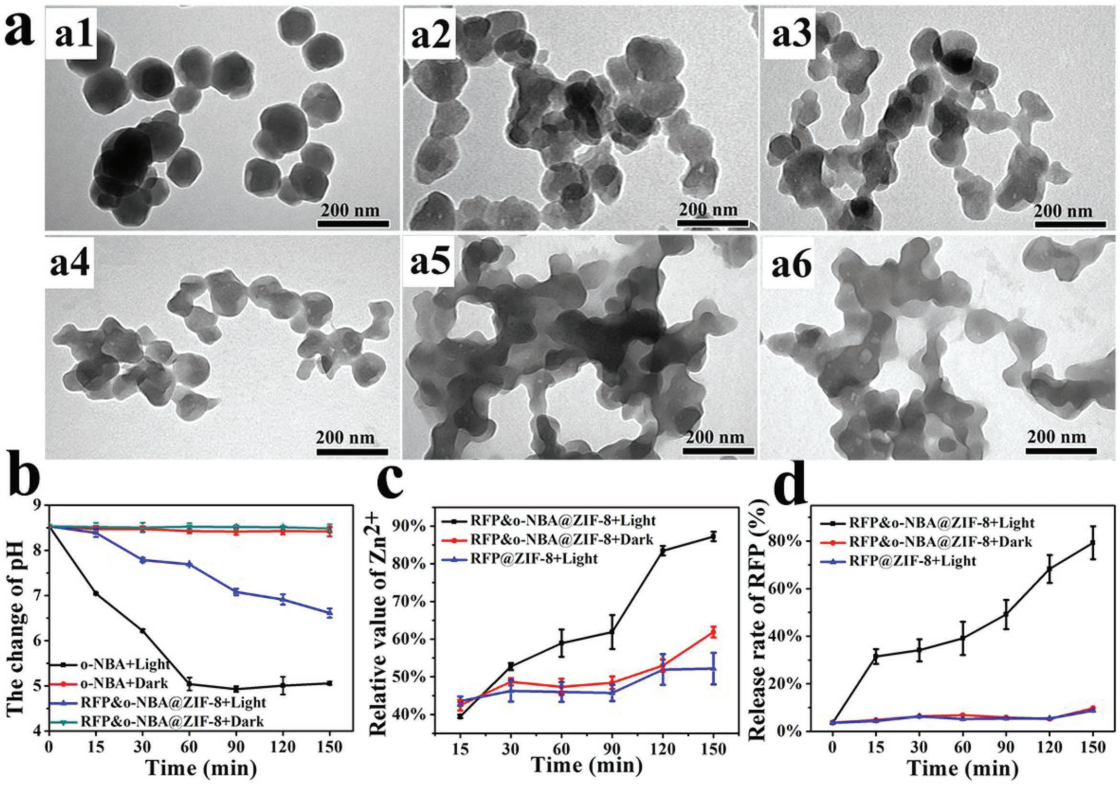

Figure 2. a) TEM of RFP&o-NBA@ZIF-8 treated with UV irradiation for different periods of time ((a1–a6) 15, 30, 60, 90, 120, 150 min). The b) pH change, c) the release efficiency of Zn^{2+}, and d) the antibiotic release efficiency after UV light treatment for different periods of time.

2.3. Light-Triggered Precise Antibiotic Release

To investigate if the light-responsive pH elevation can control the antibiotic release behavior of the RFP&o-NBA@ZIF-8, we prepared an RFP@ZIF-8 without o-NBA as a control. These solutions were then exposed to UV-light (365 nm) irradiation for a different time. The precise control of drug release was demonstrated by monitoring the effect and the content of the released antibiotic drug after alternating periods of exposure to UV light and dark conditions as shown in Figure 2d and Figures S11 and S12 (Supporting Information). In the antibiotic release profile of the RFP@ZIF-8, almost no antibiotic was detected, but in the RFP&o-NBA@ZIF-8, a maximum of 80 wt% of antibiotic was detected at 150 min under UV light exposure, indicating an apparent dependence of the release rate on the external light stimuli. Under dark conditions, only a small amount of antibiotic was released over a long duration (Figure S13, Supporting Information). These results revealed that the light-responsive acid generation can decompose the ZIF-8 MOF structure, leading to antibiotic release. More importantly, the antibiotic release can only be triggered by 365 nm light exposure and the release amount was highly dependent on the time of light exposure, thus realizing "UV light-triggered precise antibiotic release."

2.4. In Vitro Antibacterial Efficacy Evaluation

The potential of RFP&o-NBA@ZIF-8 for antibacterial applications was evaluated using several bacterial strains, such as MRSA, and Ampicillin-resistant *Escherichia coli* and *Escherichia coli* (*E. coli*). MRSA, one of the main dreaded clinical pathogens (superbugs) that cause life-threatening diseases such as sepsis and acute endocarditis, accounts for numerous cases of morbidity and mortality clinically.[25] Rifampicin (RFP) is one of the most potent and broad-spectrum antibiotics for treatment of tuberculosis (TB), leprosy and a growing number of Gram-positive bacteria such as multidrug-resistant *S. aureus*.[26] RFP diffuses freely into tissues, living cells, and bacteria, making it extremely effective against intracellular pathogens.[27] The antibacterial activity was evaluated separately by the spread plate method and a growth-inhibition assay in liquid medium (**Figure 3**). Seven different samples were used to study the antibacterial activities against the Gram-negative ampicillin-resistant *E. coli* with a series of concentrations (0–80 μg mL^{-1}) under different illumination time (0–150 min) (Figure S14, Supporting Information). The survival rates of bacteria were found to decrease with an increase of the concentration of nanocomposites and illumination time, and 10 μg mL^{-1} and 120 min illumination time were chosen as the optimum

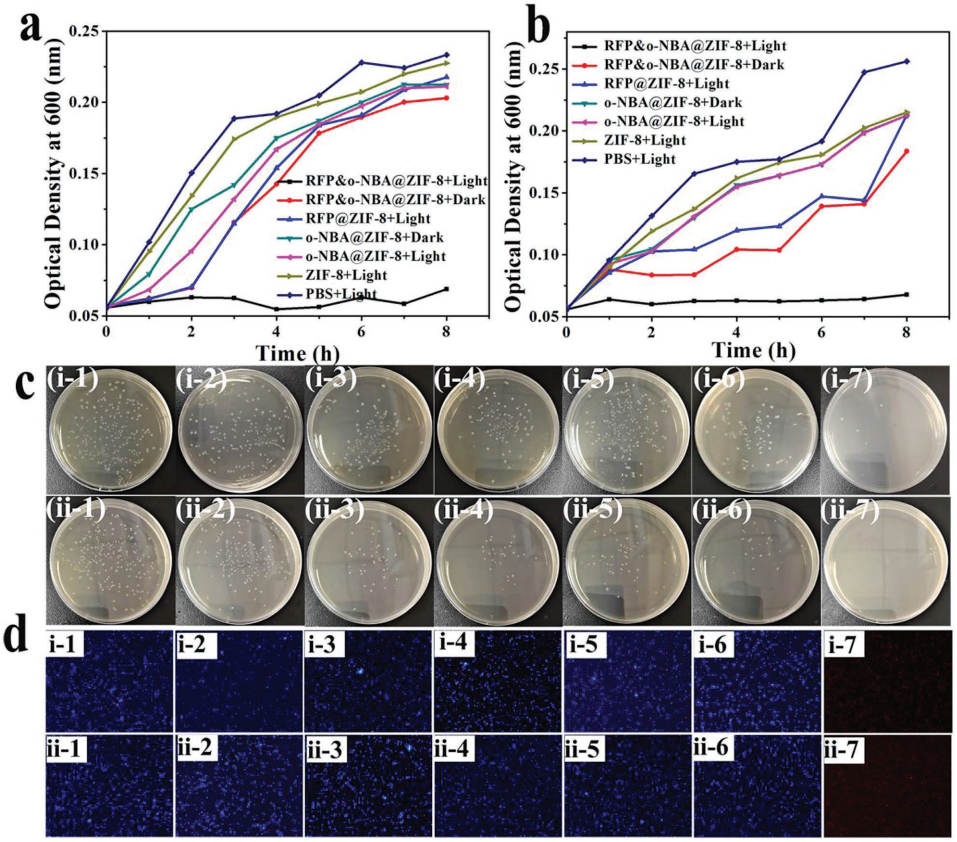

Figure 3. The optical density at 600 nm (OD600) of a) ampicillin-resistant *Escherichia coli* and b) MRSA after treatment with 10 μg mL^{-1} of materials under different conditions. c) Coated flat panel and d) live/dead staining of i) Ampicillin-resistant *Escherichia coli* and ii) MRSA treated under different conditions: 1) PBS + Light, 2) ZIF-8 + Light, 3) o-NBA@ZIF-8 + Dark, 4) o-NBA@ZIF-8 + Light, 5) RFP@ZIF-8 + Light, 6) RFP&o-NBA@ZIF-8 + Dark, and 7) RFP&o-NBA@ZIF-8 + Light.

conditions. Comparatively, the RFP&o-NBA@ZIF-8 sample exhibited an obviously higher antibacterial activity against the Gram-negative ampicillin-resistant *E. coli* and Gram-positive MRSA than an equal amount of any other samples under light treatment. However, it showed no obvious inhibition on the bacterial growth under dark treatment (Figure 3a,b). Similar results were also observed in the spread plate assay (Figure 3c). Moreover, the live/dead bacterial staining assay confirmed the direct bactericidal effect of the nanocomposite (Figure 3d). These phenomena were accordant with the fact that, in order to disrupt the ZIF-8 structure, the o-NBA can change the pH of the environment when undergoing intramolecular ESHT upon light irradiation,[28] leading to the controlled release of a larger amount of antibiotic and Zn^{2+} (Figure 1b–d). Meanwhile, the RFP has a broad-spectrum antimicrobial activity,[27] and the release of Zn^{2+} from ZnO is suggested as one of the primary antibacterial mechanisms of ZnO NPs.[29] The antimicrobial activity of metal nanomaterials is concentration-dependent. Zinc ions can show toxic effects at high concentrations, but the minimum inhibitory concentrations of zinc ions for *S. aureus* were reported in the $2–20 \times 10^{-3}$ M range (65–131 mg L^{-1}). In Vitro antibacterial assay had similar results to those of previous experimental (Figure S15, Supporting Information). Therefore, a synergistic effect between antibiotic and Zn^{2+} was proposed as a possible pathway that plays an important role in the antimicrobial activity of RFP&o-NBA@ZIF-8.

2.5. In Vivo Antibacterial Efficacy and Bacterial Infection Combination Therapy

The treatment of wound infection with this antibacterial design was demonstrated using the injury model that was fabricated on the back of mice. The back of BALBc mice (6–8 weeks) was slashed and injected with 1×10^6 of MRSA cells and ampicillin-resistant *Escherichia coli* to construct the infected wound model. The mice were divided into seven groups according to the seven separate treatments with 1) PBS + Light, 2) ZIF-8 + Light, 3) o-NBA@ZIF-8 + Light, 4) o-NBA@ZIF-8 + Dark, 5) RFP@ZIF-8, 6) RFP&o-NBA@ZIF-8 + Dark, 7) RFP&o-NBA@ZIF-8 + Light. To assess the bactericidal effect, we excised the wound tissues and collected the blood to quantify the number of bacteria in them (**Figure 4**). From the grown colonies, we could see that RFP&o-NBA@ZIF-8+Light showed the most effective wound antibacterial therapy among the seven treatments (Figure 4a,b; Figure S16a,b, Supporting Information). Meanwhile, it significantly removed the bacteria in the blood (Figure 4c,d; Figure S16c,d, Supporting Information). Moreover, the healing ability of mice in wound-infecting bacterial skin was evaluated by histological analysis. As shown in **Figure 5**a and Figure S17a (Supporting Information), a large amount of inflammatory cells appeared on the wound under the six control treatments, while less inflammatory cells emerged on the wound under the 3-d RFP&o-NBA@ZIF-8+Light treatment. Masson's trichrome staining was used to verify the formation of collagen fiber (blue) during the wound healing process (Figure 5b; Figure S17b, Supporting Information). Unrepaired collagen fibers were observed in the samples under the six control treatments, whereas well established collagen fibers and dermal layer were found in the samples under the RFP&o-NBA@ZIF-8+Light treatment. The wound size under the synergistic treatment decreased (80%) rapidly relative to the other six treatments (Figure 5c; Figures S17c and S18, Supporting Information). These results demonstrate that the RFP&o-NBA@ZIF-8+Light treatment can effectively kill bacteria, promote scar generation to protect the wound tissue, and further modulate the collagen alignment.

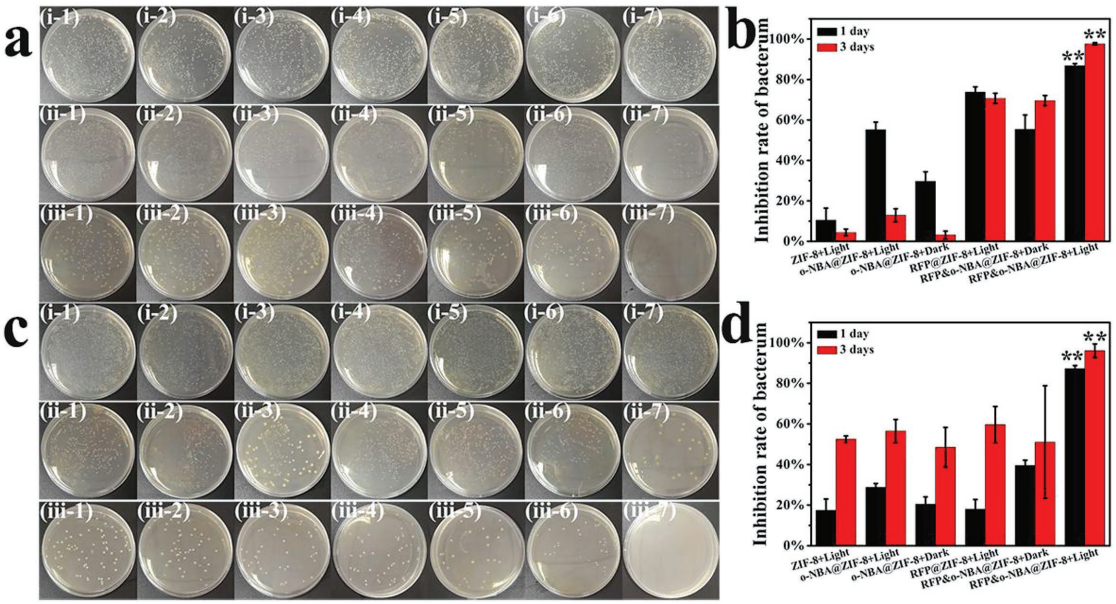

Figure 4. a,c) Coated flat panel, b,d) inhibition rate of MRSA at a,b) wound and c,d) blood treated with 1) PBS + Light, 2) ZIF-8 + Light, 3) o-NBA@ZIF-8 + Dark, 4) o-NBA@ZIF-8 + Light, 5) RFP@ZIF-8 + Light, 6) RFP&o-NBA@ZIF-8 + Dark, 7) RFP&o-NBA@ZIF-8 + Light i) 0 d (infected for 12 h), ii) 1 d, iii) 3 d. The bacteria infected for 12 h were diluted 10^4 times before coating plates. The bacteria for first and third days were diluted 10^2 times before coating plates (**$P < 0.01$).

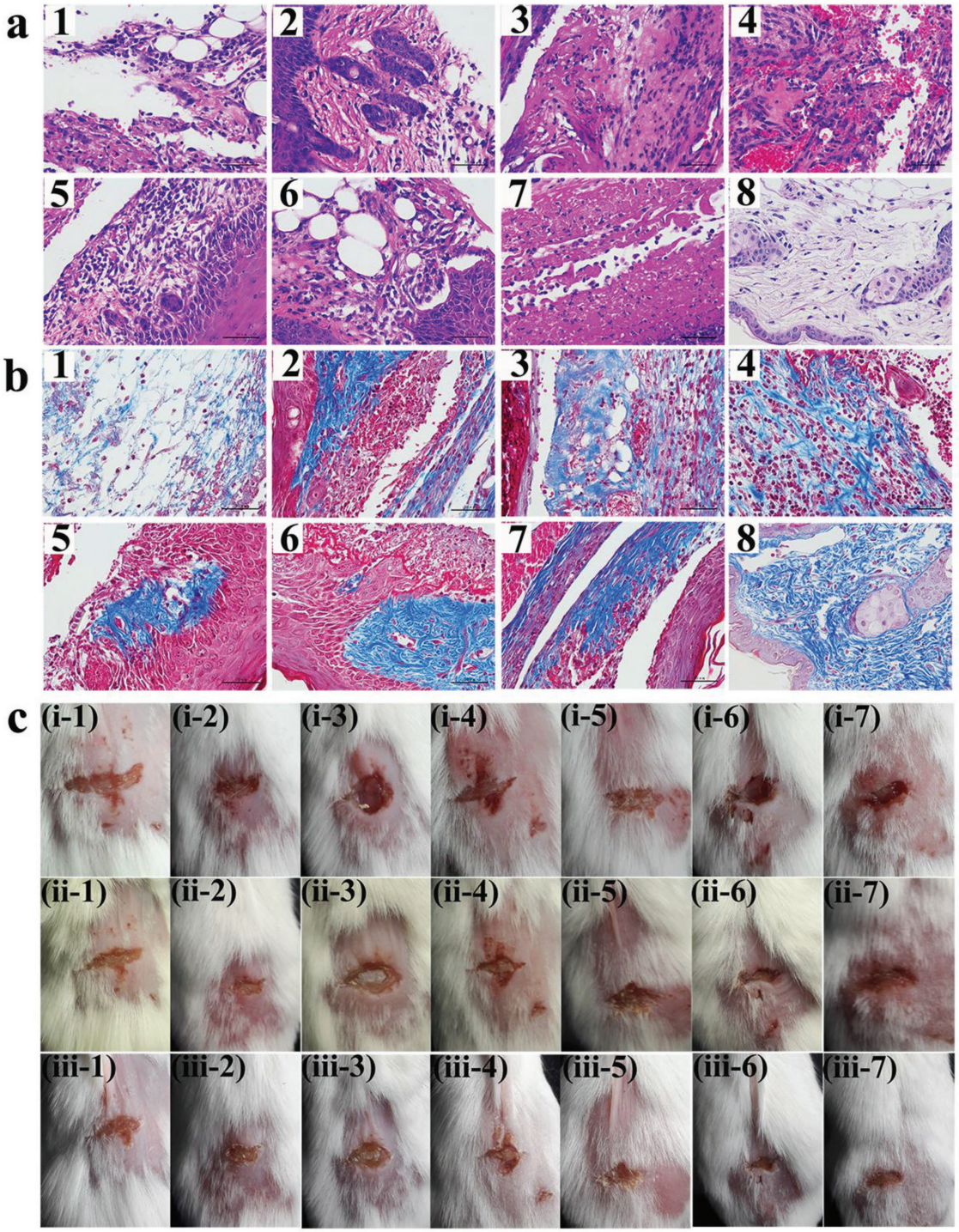

Figure 5. The images of a) H&E and b) masson and c) photographs of infected wound infected by MRSA 1) PBS + Light, 2) ZIF-8 + Light, 3) o-NBA@ZIF-8 + Dark, 4) o-NBA@ZIF-8 + Light, 5) RFP@ZIF-8 + Light, 6) RFP&o-NBA@ZIF-8 + Dark, 7) RFP&o-NBA@ZIF-8 + Light, 8) healthy mice. i) 0 d (infected for 12 h), ii)1 d, iii) 3 d.

3. Conclusion

In summary, a light-triggered gatekeeper system for spatiotemporal antibiotic release has been demonstrated. The key mechanism for the gatekeeper is the light-initiated sequential reaction. In this reaction, illumination induces acid generation by activating the pH jump reagent, which degrades the MOF and leads to the controlled release of antibiotic and zinc ions. This rational design was successfully used to develop a light-responsive antibiotic-delivery system, and its therapeutic

potential on the wound infection was also demonstrated. Further in vivo studies are currently ongoing in our laboratory.

4. Experimental Section

Materials and Reagents: Zinc nitrate hexahydrate ($ZnNO_3{\cdot}6H_2O$), HmIm, o-NBA, RFP, and Zincon ($C_{20}H_{15}N_4NaO_6S$) were purchased from Aladdin Industrial Corporation (Shanghai, China). Propidium iodide (PI) and 4′-6-diamidino-2-phenylindole (DAPI) products were purchased from Beyotime Institute of Biotechology (Shanghai, China). 365 nm UV lamp was purchased from TOSHIBA Corporation. 4% paraformaldehyde PBS was purchased from Wuhan Google Biotechnology Co., Ltd. The BABL/c mice were purchased from Hubei Experimental Animal Research Center (Permit number: SCXK 2015-0018).

Synthesis of ZIF-8: The 2-methylimidazole solution was slowly added dropwise into the zinc nitrate solution at room temperature under stirring for 30 min.[18a,30] After the reaction, the mixture was washed twice with deionized water and then freeze-dried. Finally, a white solid was obtained.

Synthesis of RFP&o-NBA@ZIF-8: Briefly, 5 mg mL^{-1} of rifampin was prepared as A solution and 5 mg mL^{-1} of 2-nitrobenzaldehyde was prepared as B solution. Then, 1.414 g of 2-methylimidazole was weighed and dissolved in 10 mL of deionized water, and 0.073 g of zinc nitrate hexahydrate was dissolved in 500 µL of deionized water. Next, 1 mL of A solution and 1 mL of B solution were added into the 2-methylimidazole solution at room temperature. Under stirring, the solution of zinc nitrate was slowly added dropwise for 30 min. After the reaction, the mixture was washed twice with deionized water and then freeze-dried. Finally, a white solid was obtained.

Synthesis of RFP@ZIF-8: The 2-methylimidazole solution was added into 1 mL of A solution at room temperature. Under stirring, the solution of zinc nitrate was slowly added dropwise for 30 min. After the reaction, the mixture was washed twice with deionized water and then freeze-dried. Finally, a white solid was obtained.

Synthesis of o-NBA@ZIF-8: The 2-methylimidazole solution was added into 1 mL of B solution at room temperature. Under stirring, the solution of zinc nitrate was slowly added dropwise for 30 min. After the reaction, the mixture was washed twice with deionized water and then freeze-dried. Finally, a white solid was obtained.

Characterization: UV–vis absorption spectra were acquired via a Nicolet Evolution 300 UV–vis spectrometer (Thermo Nicolet, United States). FT-IR spectra were obtained on a Nicolet Avatar-330 spectrometer with 4 cm^{-1} resolution using the KBr pellet. The ζ potential was measured by DLS using a Malvern Zeta sizer (Nano-ZS) system. TEM images were taken with a JEM-2010 transmission electron microscope. Fluorescence imaging was taken with fluorescent microscopy (Nikon, Japan). The optical density (OD) value was measured by a microplate reader. All the photos were taken with a Canon camera.

Detection of Zinc Ions: RFP&o-NBA@ZIF-8 and RFP@ZIF-8 (2 mg mL^{-1}) solutions were exposed to UV light (365 nm) or dark conditions for a different period of time (15, 30, 60, 90, 120, 150 min). These solutions were centrifuged by 10 000 rpm for 8 min to collect the supernatant. Finally, 100 µL of the supernatant was detected by a zinc reagent.

Detection of pH: The pH was adjusted to 8.5 for the RFP&o-NBA@ZIF-8 solution (1 mg mL^{-1}) and free o-NBA solution (0.055 mg mL^{-1}). Next, the solutions were exposed to UV light (365 nm) or dark conditions for a different period of time (15, 30, 60, 90, 120, 150 min) and the pH value at different time points was measured by an Orion portable pH meter connected with an PHS-3C pH electrode (Shanghai *INESA* Scientific Instrument CO.LTD China).

Bacterial Culture: Gram-negative *E. coli* (AB 93154) was acquired from China Centre For Type Culture Collection. MRSA (1213P46B) was isolated from nasal swabs of clinical pigs, and ampicillin-resistant *E. coli* (PCN033) was isolated from the brain tissue of pigs with clinical symptoms. The bacteria were cultured in Luria–Bertani broth medium (LB) and harvested at the exponential growth phase prior to experiments. The concentration of bacteria was monitored by measuring the OD at a wavelength of 600 nm.

Antibacterial Experiments: The antimicrobial activity of the materials was evaluated by examining the OD600 growth curves as follows. To explore the optimum concentration of the material and the optimum time for UV irradiation (λ = 365 nm), *E. coli* cells treated with different materials and different concentrations were grown in LB broth at 30 °C for 12 h under 120 rpm rotation and were harvested to create the growth curve. The cells were collected by centrifugation at 3000 rpm for 3 min, then the cells were resuspended in water and adjusted to 10^8 cfu mL^{-1}. Next, 1 mL cell suspension and 1 mL RFP&o-NBA@ZIF-8 and RFP@ZIF-8 with a different concentration (5, 10, 20, 40, 80 µg mL^{-1}) were mixed and incubated under UV irradiation or in the dark. Control samples containing 1 mL of the cells suspension were mixed with 1 mL of deionization (DI) water. After irradiation at different times (15, 30, 60, 90, 120, 150 min), 200 µL of each treated bacteria was transferred into 20 mL LB broth. The *E. coli* cells were then incubated at 30 °C in an incubator under constant agitation at 120 rpm. Growth rates and bacterial concentrations were determined by measuring the optical density (OD600) at the indicated time interval.

Different experimental groups were established to explore the antibacterial effect of different materials against the ampicillin-resistant *E. coli* and MRSA. The experimental groups were 1) PBS + Light, 2) ZIF-8 + Light, 3) o-NBA@ZIF-8 + Light, 4) o-NBA@ZIF-8 + Dark, 5) RFP@ZIF-8, 6) RFP&o-NBA@ZIF-8 + Dark, 7) RFP&o-NBA@ZIF-8 + Light. First, the growth curve of *E. coli* and *S. aureus* was detected under the concentration of 10 µg mL^{-1} and the irradiation time of 2 h. In order to measure the bacterial mortality, the bacteria treated were diluted and uniformly coated in LB solid medium and left to grow for 24 h at 30 °C. Colony forming unit (CFU) was counted and compared with the control plate to calculate the death rate. Each treatment was prepared in triplicate and the mean values were compared.

Live/Dead Staining Assay: In order to gain a more intuitive performance of the bactericidal effect, live/dead staining assay was performed. The bacteria cells were stained with PI (100 µg mL^{-1}) and DAPI for 15 and 5 min in the dark, respectively. Fluorescence images were taken on an Olympus BX40 fluorescence microscope during a single batch experiment at 400× magnification.

MTT Assay: MTT assays were performed to investigate ZIF complex cytotoxicity. Hela cells (1×10^6 cells per well) were washed twice with PBS and incubated with serial concentrations of RFP&o-NBA@ZIF-8, RFP@ZIF-8, o-NBA@ZIF-8, ZIF-8 for 2 h, cells incubated with only the PBS was used as control. The optical density at a wavelength of 490 nm was measured with a Perkin Elmer microplate reader, and the results showed that these materials do not have any toxicity to the cells. According to previous experimental results, the mouse wounds were treated dropwise with 10 µL, and 80 µg mL^{-1} of different materials, and then stood for 2 h under UV light or dark conditions.

Mice Injury Model: To evaluate the potential of the RFP&o-NBA@ZIF-8 for treating wound infection under the UV light (λ = 365 nm), the injury model was established on the BALB/c mice (6–8 weeks).[31] The back of the mice was slashed and injected with 100 µL of 1×10^6 CFU mL^{-1} of MRSA or ampicillin-resistant *E. coli* to build the infected wound model. All the mice were randomly divided into seven groups, six mice per group, and named as 1) PBS + Light, 2) ZIF-8 + Light, 3) o-NBA@ZIF-8 + Light, 4) o-NBA@ZIF-8 + Dark, 5) RFP@ZIF-8, 6) RFP&o-NBA@ZIF-8 + Dark, and 7) RFP&o-NBA@ZIF-8 + Light. After 12 h infection, three mice were randomly selected from each group and then the bacteria were collected by swabbing in the mice wound using the cotton swab and taking the blood of the tail vein. Bacteria were counted by plate dilution. After establishing the infection, the mice in different groups were treated separately with PBS buffer only, 10 µL of 80 µg mL^{-1} ZIF-8, o-NBA@ZIF-8, RFP@ZIF-8, and RFP&o-NBA@ZIF-8 on the wound, then stood for 2 h under UV light irradiation or dark conditions. The wound was observed and photographed every day. Finally, the bacteria were harvested at the wound in the same way on the first and third days and then counted.

Histology: For histology, the mice were sacrificed, and the wound tissues were harvested after 3 d of therapy. The wound tissues treated with different nanoparticles were fixed in 4% paraformaldehyde PBS buffer and stained with H&E and masson. The samples were examined in Wuhan Google Biotechnology Co., Ltd.

Disposal of the Experimental Mice: In order to reduce the impact of experimental mice on the environment, the wound tissues were harvested and the experimental mice were collected and sterilized.

Statistical Analyses: The statistical significance of antibacterial activity differences among different groups was analyzed using Student's *t*-test in SPSS software (*$p < 0.05$, **$p < 0.01$, ***$p < 0.001$, ns, not significant). The results with error bars are expressed as means ± standard deviations.

Supporting Information

Supporting Information is available from the Wiley Online Library or from the author.

Acknowledgements

Z.Y.S. and Y.W. contributed equally to this work. This work was financially supported by the Funded by National Natural Science Foundation of China (21375043, 21778020), the Fundamental Research Funds for the Central Universities (2662016QD027). The authors are also thankful to Prof. Hanchang Zhu and Dr. Xiaoyu Wang for editing of the language.

Conflict of Interest

The authors declare no conflict of interest.

Keywords

antibiotics, controlled release, light triggers, synergistic antibacterial, zeolitic imidazolate frameworks

Received: January 1, 2018
Revised: March 2, 2018
Published online:

[1] a) Q. Zhang, G. Lambert, D. Liao, H. Kim, K. Robin, C. K. Tung, N. Pourmand, R. H. Austin, *Science* **2011**, *333*, 1764; b) C. M. Courtney, S. M. Goodman, J. A. McDaniel, N. E. Madinger, A. Chatterjee, P. Nagpal, *Nat. Mater.* **2016**, *15*, 529.

[2] a) S. Mura, J. Nicolas, P. Couvreur, *Nat. Mater.* **2013**, *12*, 991; b) H. Yan, C. Teh, S. Sreejith, L. Zhu, A. Kwok, W. Fang, X. Ma, K. T. Nguyen, V. Korzh, Y. Zhao, *Angew. Chem., Int. Ed.* **2012**, *51*, 8373.

[3] a) Y. H. Wang, S. Y. Song, J. H. Liu, D. P. Liu, H. J. Zhang, *Angew. Chem., Int. Ed.* **2015**, *54*, 536; b) H. J. Yu, Z. R. Cui, P. C. Yu, C. Y. Guo, B. Feng, T. Y. Jiang, S. L. Wang, Q. Yin, D. F. Zhong, X. L. Yang, Z. W. Zhang, Y. P. Li, *Adv. Funct. Mater.* **2015**, *25*, 2489; c) H. L. Pu, W. L. Chiang, B. Maiti, Z. X. Liao, Y. C. Ho, M. S. Shim, E. Y. Chuang, Y. N. Xia, H. W. Sung, *ACS Nano* **2014**, *8*, 1213.

[4] S. Ganta, H. Devalapally, A. Shahiwala, M. Amiji, *J. Controlled Release* **2008**, *126*, 187.

[5] a) Z. Wang, X. Tang, X. Wang, D. Yang, C. Yang, Y. Lou, J. Chen, N. He, *Chem. Commun.* **2016**, *52*, 12210; b) J. W. Xu, X. M. Zhou, Z. D. Gao, Y. Y. Song, P. Schmuki, *Angew. Chem., Int. Ed.* **2016**, *55*, 593.

[6] a) R. de la Rica, D. Aili, M. M. Stevens, *Adv. Drug Delivery Rev.* **2012**, *64*, 967; b) P. D. Thornton, R. J. Mart, R. V. Ulijn, *Adv. Mater.* **2007**, *19*, 1252.

[7] a) N. Kamaly, B. Yameen, J. Wu, O. C. Farokhzad, *Chem. Rev.* **2016**, *116*, 2602; b) Z. Fan, L. M. Sun, Y. J. Huang, Y. Z. Wang, M. J. Zhang, *Nat. Nanotechnol.* **2016**, *11*, 388.

[8] Y. Jiang, J. Chen, C. Deng, E. J. Suuronen, Z. Zhong, *Biomaterials* **2014**, *35*, 4969.

[9] Y. Lvov, W. C. Wang, L. Q. Zhang, R. Fakhrullin, *Adv. Mater.* **2016**, *28*, 1227.

[10] H. Wei, R. X. Zhuo, X. Z. Zhang, *Prog. Polym. Sci.* **2013**, *38*, 503.

[11] a) L. H. Li, Z. Li, W. Shi, X. H. Li, H. M. Ma, *Anal. Chem.* **2014**, *86*, 6115; b) Z. Li, X. H. Gao, W. Shi, X. H. Li, H. M. Ma, *Chem. Commun.* **2013**, *49*, 5859.

[12] a) H. Zheng, Y. Zhang, L. Liu, W. Wan, P. Guo, A. M. Nystrom, X. Zou, *J. Am. Chem. Soc.* **2016**, *138*, 962; b) I. Imaz, J. Hernando, D. Ruiz-Molina, D. Maspoch, *Angew. Chem., Int. Ed.* **2009**, *48*, 2325.

[13] a) C. B. He, D. M. Liu, W. B. Lin, *Chem. Rev.* **2015**, *115*, 11079; b) Y. Yang, J. Liu, C. Liang, L. Feng, T. Fu, Z. Dong, Y. Chao, Y. Li, G. Lu, M. Chen, Z. Liu, *ACS Nano* **2016**, *10*, 2774; c) Y. Liu, S. Y. Moon, J. T. Hupp, O. K. Farha, *ACS Nano* **2015**, *9*, 12358.

[14] a) M. Eddaoudi, D. B. Moler, H. L. Li, B. L. Chen, T. M. Reineke, M. O'Keeffe, O. M. Yaghi, *Acc. Chem. Res.* **2001**, *34*, 319; b) H. L. Jiang, B. Liu, T. Akita, M. Haruta, H. Sakurai, Q. Xu, *J. Am. Chem. Soc.* **2009**, *131*, 11302.

[15] T. Rodenas, I. Luz, G. Prieto, B. Seoane, H. Miro, A. Corma, F. Kapteijn, I. X. F. X. Llabres, J. Gascon, *Nat. Mater.* **2015**, *14*, 48.

[16] J. Guo, Y. Li, Y. Cheng, L. Dai, Z. Xiang, *ACS Nano* **2017**, *11*, 8379.

[17] a) Q. Yang, Q. Xu, S. H. Yu, H. L. Jiang, *Angew. Chem., Int. Ed.* **2016**, *55*, 3685; b) W. W. Zhan, Q. Kuang, J. Z. Zhou, X. J. Kong, Z. X. Xie, L. S. Zheng, *J. Am. Chem. Soc.* **2013**, *135*, 1926.

[18] a) K. Liang, R. Ricco, C. M. Doherty, M. J. Styles, S. Bell, N. Kirby, S. Mudie, D. Haylock, A. J. Hill, C. J. Doonan, P. Falcaro, *Nat. Commun.* **2015**, *6*, 7240; b) J. Zhuang, C. H. Kuo, L. Y. Chou, D. Y. Liu, E. Weerapana, C. K. Tsung, *ACS Nano* **2014**, *8*, 2812.

[19] L. Yan, X. Chen, Z. Wang, X. Zhang, X. Zhu, M. Zhou, W. Chen, L. Huang, V. A. L. Roy, P. K. N. Yu, G. Zhu, W. Zhang, *ACS Appl. Mater. Interfaces* **2017**, *9*, 32990.

[20] L. Palanikumar, E. S. Choi, J. Y. Cheon, S. H. Joo, J. H. Ryu, *Adv. Funct. Mater.* **2015**, *25*, 957.

[21] a) C. L. Zhu, C. H. Lu, X. Y. Song, H. H. Yang, X. R. Wang, *J. Am. Chem. Soc.* **2011**, *133*, 1278; b) W. P. Fan, W. B. Bu, Z. Zhang, B. Shen, H. Zhang, Q. J. He, D. L. Ni, Z. W. Cui, K. L. Zhao, J. W. Bu, J. L. Du, J. N. Liu, J. L. Shi, *Angew. Chem., Int. Ed.* **2015**, *54*, 14026.

[22] S. S. Wu, X. Huang, X. Z. Du, *Angew. Chem., Int. Ed.* **2013**, *52*, 5580.

[23] Y. Hu, H. Kazemian, S. Rohani, Y. N. Huang, Y. Song, *Chem. Commun.* **2011**, *47*, 12694.

[24] S. Kohse, A. Neubauer, A. Pazidis, S. Lochbrunner, U. Kragl, *J. Am. Chem. Soc.* **2013**, *135*, 9407.

[25] a) X. Li, S. M. Robinson, A. Gupta, K. Saha, Z. Jiang, D. F. Moyano, A. Sahar, M. A. Riley, V. M. Rotello, *ACS Nano* **2014**, *8*, 10682; b) Z. Zhao, R. Yan, X. Yi, J. Li, J. Rao, Z. Guo, Y. Yang, W. Li, Y. Q. Li, C. Chen, *ACS Nano* **2017**, *11*, 4428.

[26] N. Maggi, C. R. Pasqualucci, R. Ballotta, P. Sensi, *Chemotherapy* **1966**, *11*, 285.

[27] E. A. Campbell, N. Korzheva, A. Mustaev, K. Murakami, S. Nair, A. Goldfarb, S. A. Darst, *Cell* **2001**, *104*, 901.

[28] H. W. Choi, J. Kim, J. Kim, Y. Kim, H. B. Song, J. H. Kim, K. Kim, W. J. Kim, *ACS Nano* **2016**, *10*, 4199.

[29] Y. W. Wang, A. Cao, Y. Jiang, X. Zhang, J. H. Liu, Y. Liu, H. Wang, *ACS Appl. Mater. Interfaces* **2014**, *6*, 2791.

[30] Y. Pan, Y. Liu, G. Zeng, L. Zhao, Z. Lai, *Chem. Commun.* **2011**, *47*, 2071.

[31] a) F. F. Cao, E. G. Ju, Y. Zhang, Z. Z. Wang, C. Q. Liu, Y. Y. Huang, K. Dong, J. S. Ren, X. G. Qu, *ACS Nano* **2017**, *11*, 4651; b) W. Yin, J. Yu, F. Lv, L. Yan, L. R. Zheng, Z. Gu, Y. Zhao, *ACS Nano* **2016**, *12*, 11000.